

Counterions at Charged Cylinders: Criticality and universality beyond mean-field

Ali Naji and Roland R. Netz

Physics Department, Technical University of Munich, 85748 Garching, Germany.

(Dated: April 2005)

The counterion-condensation transition at charged cylinders is studied using Monte-Carlo simulation methods. Employing logarithmically rescaled radial coordinates, large system sizes are tractable and the critical behavior is determined by a combined finite-size and finite-ion-number analysis. Critical counterion localization exponents are introduced and found to be in accord with mean-field theory both in 2 and 3 dimensions. In 3D the heat capacity shows a universal jump at the transition, while in 2D, it consists of discrete peaks where single counterions successively condense.

PACS numbers: 64.60.Fr, 82.35.Rs, 87.15.-v, 61.20.Ja

Many biopolymers, such as DNA, actin, tubulin, filoviruses, are charged and stiff. On length scales smaller than the persistence length, they can be represented by straight, charged cylinders and oppositely charged ions (counterions) are attracted via an electrostatic potential that grows logarithmically with radial distance. As the ion conformation entropy also exhibits a logarithmic dependence, it was suggested early by Onsager that a counterion delocalization transition occurs at a critical cylinder charge (or equivalently at a critical temperature) [1]. This argument is strictly valid only for a single ion since it neglects cooperativity due to inter-ionic repulsions. Nevertheless, it was corroborated by mean-field (MF) studies [2, 3], which demonstrate that below a critical temperature, a fraction of counterions stays bound or condensed in the vicinity of the central cylinder even in the limit of infinite system size; while above the critical temperature, all counterions de-condense to infinity. This counterion-condensation transition (CCT) dramatically affects a whole number of static and dynamic quantities for charged polymers [1]. It has been observed with different polymers by varying the medium dielectric constant [4, 5] or the polymer charge density [5, 6]; the counterion distribution around DNA strands has been directly measured recently using anomalous scattering techniques [7]. Since its discovery, the CCT has been at the focus of numerical [8, 9] and analytical [10] studies. Under particular dispute has been the connection between CCT and the celebrated Kosterlitz-Thouless transition of logarithmically interacting particles in 2 dimensions [11]. Also, the precise location of the CCT critical point remains subject of ongoing experimental investigations [5, 6].

As is well known from bulk critical phenomena, fluctuations and correlations typically make non-universal and universal quantities deviate from mean-field theory (MFT) below the upper critical dimension [12]. Surprisingly, the MFT prediction for the CCT critical temperature has not been questioned in literature and apparently assumed to be exact. Likewise, the existence of scaling relations and critical exponents associated with the CCT has not been considered, neither on the MFT level and (consequently) also not in the presence of correlations.

In this paper we pose the questions: i) what is the critical temperature of the CCT, and ii) what are the associated relevant critical exponents? We employ Monte-Carlo simulations, which are performed in rescaled logarithmic coordinates in order to handle very large systems (where the criticality actually occurs) with tractable equilibration times. A combined finite-size and finite-ion-number analysis yields the desired critical temperature and exponents. To enhance the effects of fluctuations, we also study a (within MFT equivalent) 2D system of logarithmically interacting charges, as applicable to an experimental system of oriented cationic and anionic polymers (e.g. DNA with polylysine [13]). Surprisingly, MFT is demonstrated to be accurate both in 3D (charged cylinder with point-like counterions) and in 2D (charged cylinder with cylindrical counterions). The critical exponents associated with the inverse counterion localization length (which plays the order parameter of the CCT) and the universal behavior of the heat capacity are determined; both quantities are experimentally accessible.

In the 3D simulations, we consider a central cylinder of radius R and uniform surface charge density σ_s (linear charge density $\lambda = 2R\sigma_s$) with N neutralizing point-like counterions of valency q confined laterally in an outer cylindrical box of radius D (see Fig. 1 for snapshots projected along the z -axis). Periodic boundary conditions in z -direction are handled using summation methods for long-range interactions [14]. Rescaling all spatial coordinates by the Gouy-Chapman length, $\lambda_B = 1/(2q\sigma_s)$, as $\mathbf{x} = \lambda_B \mathbf{x}'$, we obtain the Hamiltonian $H = 2 \sum_{i=1}^N \ln(\epsilon_i/R) + \sum_{hi,ji} 1/\epsilon_i \epsilon_j$ (per $k_B T$), where $\lambda_B = e^2/(4\pi\epsilon_0 k_B T)$ is the Bjerrum length, and ϵ is the radial distance from the cylinder axis. The coupling parameter, $\beta = 2q^3 \lambda_B^2 \sigma_s$, is an indicator for the importance of ionic correlations: in the limit $\beta \rightarrow 0$, correlations are unimportant and MFT becomes exact; in the converse strong-coupling limit $\beta \rightarrow \infty$, MFT breaks down [15]. The so-called Manning parameter (rescaled inverse temperature), $\nu = q\lambda_B$, regulates the CCT and is a measure of counterion binding: According to MFT [1, 2, 3], the CCT occurs for $\nu = \ln(D/R) + 1$ at the MF critical threshold

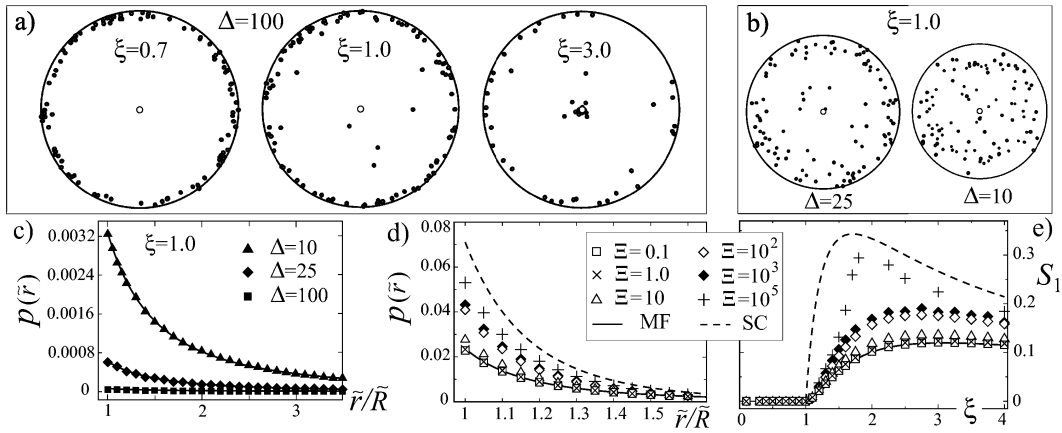


FIG. 1: Snapshot-topviews for a) logarithmic box radius $\Delta = \ln(D/R) = 100$ and Manning parameters $\xi = 0.7; 1.0$ and 3.0 , and b) $\xi = 1.0$ and $\Delta = 10$ and 25 shown in logarithmic radial units $y = \ln(r/R)$ (number of particles $N = 100$ and the coupling parameter $\beta = 0.1$). c) Radial counterion distribution function, $p(r)$, for $\xi = 1.0$, $\beta = 0.1$, $N = 100$ and various system sizes. d) Counterion distribution for $\xi = 3.0$ and various Δ shows a crossover between MFT (solid curve) and SC (dashed curve) predictions, Eqs. (2) and (3). e) Order parameter $S_1 = \langle |r|^{-1} \rangle$ as a function of Manning parameter, ξ , for different coupling parameters compared with MFT (solid curve) and SC (dashed curve) results, Eqs. (4) and (5). In d), e) $\beta = 300$ and typically $N = 200$.

$M^F = 1$, above which a fraction $1 - M^F$ of counterions condenses. To investigate the critical limit for large lateral system size, we introduce a (centrifugal) sampling method by mapping the radial coordinate to the logarithmic scale as $y = \ln(r/R)$. The partition function transforms as $Z = \int \prod_i dz_i d\phi_i \exp(-H)$ $\int \prod_i dy_i dz_i d\phi_i \exp(-H_{MC})$, where the Hamiltonian

$$H_{MC} = 2 \sum_{i=1}^N \ln \frac{r_i}{R} + \sum_{i,j=1}^N \frac{q_i q_j}{h_{ij}} \quad (1)$$

is used for Monte-Carlo sampling; it features a linear potential (1st term) acting on counterions from competing energetic (2y) and entropic or centrifugal (2y) contributions associated with the cylindrical boundary.

In Fig. 1a, we show the snapshot-topviews from our simulations for $\Delta = \ln(D/R) = 100$. De-condensation phase is reproduced for small Manning parameter, $\xi = 0.7$, as counterions gather at the outer boundary; while for $\xi = 3$, a fraction of counterions accumulates or condenses around the central cylinder. The transition regime for intermediate ξ exhibits strong finite-size effects: As seen for $\xi = 1$ in Figs. 1a and b, only for large logarithmic system size, $\Delta \gg 1$, does de-condensation occur. This is also demonstrated by vanishing radial distribution function of counterions, $p(r)$, for growing Δ in Fig. 1c. For small coupling parameter $\beta = 0.1$, the data for $p(r)$ compare well with the normalized MFT profile (solid curves)

$$p_{MF}(r) = \frac{2}{2 - \xi^2} \sin^2 \left[\ln \frac{r}{R} + \cot^{-1} \frac{1}{\xi} \right]; \quad (2)$$

where $\xi = (1 + \beta)$ and β is given by $\beta = (1 + \beta^2) = (1 + \cot^2(\beta))$ [2]. Conversely, for large coupling $\beta \gg 1$,

strong-coupling (SC) theory [15] becomes valid and yields

$$p_{SC}(r) = \frac{2}{2 - \xi^2} \frac{1}{r} e^{2(1 - \xi^2) \ln \frac{r}{R}}; \quad (3)$$

The break-down of MFT for increasing coupling parameter is demonstrated in Fig. 1d (at $\xi = 3$), where the distribution function exhibits a gradual crossover between the asymptotic MFT and SC predictions [15]. Enhanced ionic correlations at elevated β cause a remarkably larger counterion density near the charged cylinder [8, 16]. The central question is whether these correlations influence the critical behavior associated with the CCT.

The standard analysis of critical behavior relies on suitably-defined order parameters [12]. Here, this role is taken by the inverse moments of the counterion distribution function, $S_n = \langle |r|^{-n} \rangle$ (with $n > 0$); S_n vanishes in the de-condensation phase, but attains a finite value in the condensation phase. The MFT distribution (2) gives

$$S_n^{MF} = \frac{2}{n+1} \int_0^Z dy e^{-ny} \sin^2 \left[y + \cot^{-1} \frac{1}{\xi} \right]; \quad (4)$$

while in the strong-coupling limit, we have from Eq. (3)

$$S_n^{SC} = \frac{2}{n} \frac{(1 - \xi^2)^{n-1}}{(2 + n)^{n-1}} \frac{e^{2(2+n)} - 1}{e^{2(1 - \xi^2)}}; \quad (5)$$

The data for S_1 (the mean inverse localization length) in Fig. 1e exhibit the condensation ($S_1 > 0$) and de-condensation ($S_1 = 0$) phases for a wide range of couplings, β . To locate the critical Manning parameter, ξ_c , a finite-size analysis is required since criticality is masked both by finite system size, Δ , and finite particle number,

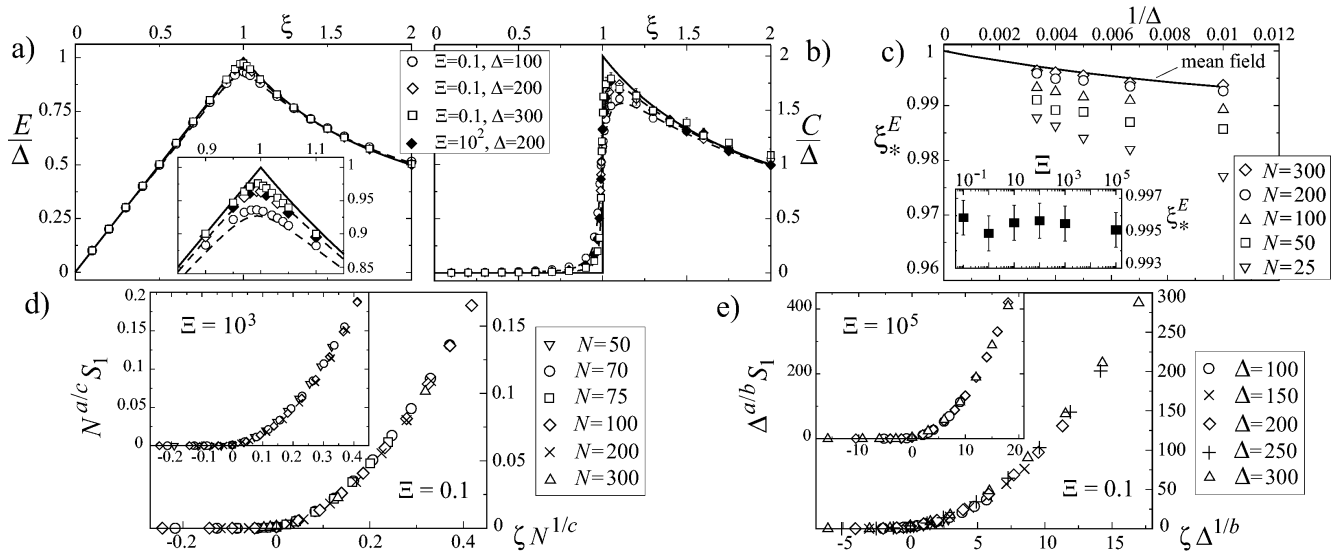


FIG. 2: a) Rescaled (potential) energy, E/Δ , and b) rescaled (excess) heat capacity, C/Δ , as a function of Manning parameter, ξ , for fixed $N = 100$ compared with the MFT prediction for $\xi \ll 1$ (solid line), $\xi = 300$ and 100 (broken lines, from top to bottom) [16]. c) Location of the peak of the energy, ξ^* , as a function of $1/\Delta$ for $\xi = 0.1$ compared with MFT (solid line); Inset: Peak location versus $1/\Delta$ for $N = 200$ and $N = 300$. d) Scale invariance of the order parameter, S_1 , near ξ_c with respect to the reduced Manning parameter, $\xi_c = 1/\Delta_c$, and the counterion number, N , with exponents $a=c=2/3$ and $1-c=1/3$ (lateral system size $\Delta = 300$). e) Scale invariance of S_1 for various Δ with exponents $a=b=2$ and $1/b=1$ ($N = 200$ is fixed).

N , in the simulations (i.e. S_1 does not vanish and saturates at a small value at critical point). To this end, we study the singular behavior of rescaled energy $E/\Delta = \langle H \rangle / (N k_B T)$ and heat capacity $C/\Delta = \langle H^2 \rangle - \langle H \rangle^2 / (N k_B T)^2 = N \langle H^2 \rangle - \langle H \rangle^2$. Simulation results for E and C (Figs. 2a, b) show a non-monotonic behavior that can be understood for large systems, $\xi \gg 1$, using a simple argument: for small ξ , all counterions are unbound and the electrostatic potential experienced by counterions is that of a bare cylinder, $\phi(r) = 2 \ln(r/R)$ (per $k_B T = eq$), at the outer boundary. The energy follows by a charging process as $E'(\xi) = 2 \ln(\xi)$. From the thermodynamic relation $\partial E / \partial \xi = E/C$, one obtains $C' = 0$. For large ξ , the cylinder potential is screened by condensed counterions. Using the MFT relation $\phi(r) = 2 \ln(r)$. A fraction $1-\xi_c$ of counterions is decondensed [1, 3, 16] and yields the leading contribution to the energy; hence $E'(\xi) = 2 \ln(\xi)$ and $C' = 2/\xi$. Thus both quantities decay with ξ as counterions become increasingly condensed. The energy exhibits a peak and the heat capacity develops a jump, which become singular for an infinite system ($\xi \gg 1, N \gg 1$) reflecting the CCT point, ξ_c (Figs. 2a, b). We determine ξ_c from the location of the energy peak, $E'(\xi; N)$, for increasing N and Δ . The numerical results for $E'(\xi; N)$ in Fig. 2c, obtained using the identity $\partial E / \partial \xi = E/C$, compare favorably with the MFT prediction (solid curve) for small coupling $\xi = 0.1$ and increasing N . The MFT prediction asymptotically tends to the MFT threshold $\xi_c^{MFT} = 1$ according to $\xi_c^{MFT} = E^{MFT}(\xi) = 1$ as $\xi \gg 1$. The location of the energy peak (and also the heat capacity

jump) shows no dependence on the coupling parameter within error bars (Fig. 2c inset). We thus find a universal counterion-condensation threshold as $\xi_c = 1.00 \pm 0.002$.

We now turn to the near-threshold scaling behavior of the order parameter. In the thermodynamic limit ($N \gg 1, \xi \gg 1$), S_n exhibits a power-law behavior as $S_n \sim \xi^{-\nu}$ (close to and above ξ_c), where $\nu = 1/\xi_c$ is the reduced Manning parameter (reduced temperature). Within MFT, we obtain $\nu_{MFT} = 2$ for all n from Eq. (4). At criticality, $\xi = 0$, one expects the scaling $S_n \sim \xi^{-\nu}$ for $N \gg 1$ but finite (within MFT, we obtain $\nu_{MFT} = 2$); while for $\xi \ll 1$ but finite N , one expects $S_n \sim N^{-\nu}$ (ξ is not defined in MFT). These relations indicate that close to criticality, $S_n(\xi; N)$ takes a homogeneous scale-invariant form, i.e. for $\xi > 0$,

$$S_n(\xi; N) = \xi^{-\nu} S_n(\xi; N) \quad (6)$$

where a, b, c are related to the exponents ν, ξ_c, N . Choosing the scale factor as $\xi = N^{1-c}$, one finds $S_n(\xi; N) = N^{-a/c} S_n(N^{1-c}; N^{b/c}; 1)$. For large N , $b/c \gg 1$, as is the case in our simulations, and at the transition, $\xi = 0$, we have $S_n \sim N^{-a/c}$ and thus obtain $\nu = a/c$. For $N \gg 1$, a similar argument leads to $S_n \sim \xi^{-a}$, which gives $\nu = a$. In Fig. 2d we plot the rescaled order parameter $N^{a/c} S_1$ as a function of N^{1-c} for various N and fixed large Δ . By choosing the scaling exponents as $\nu = a/c = 2/3$ and $1-c = 1/3$, we obtain excellent data collapse both for small coupling (main figure) and large (inset). Choosing $\xi = N^{1-b}$ in Eq. (6) yields the relation $S_n(\xi; N) = N^{-a/b} S_n(N^{1-b}; N^{c/b}; 1)$. In Fig. 2e we plot $N^{a/b} S_1$ versus N^{1-b} . Good data collapse is obtained

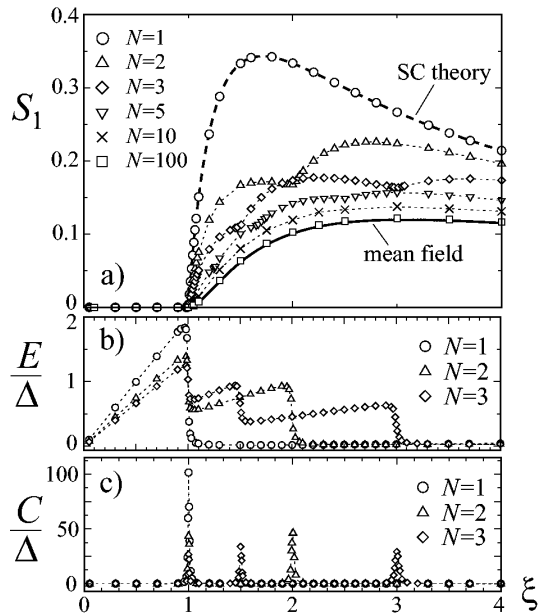


FIG. 3: 2D results: a) Order parameter $S_1 = \langle h_i = r_i \rangle$ as a function of Manning parameter, ξ , for different particle numbers, N , compared with MF and SC predictions, Eqs. (4) and (5). b) Rescaled energy and c) heat capacity (per particle) exhibit a set of singularities corresponding to successive condensation of single counterions for increasing ξ . Here $\beta = 300$.

for $\beta = a = b = 2$ (0.6 both at small (main figure) and large (inset), which also demonstrates approximate independence from the scaling argument $N^{-c=b}$ [16]. Our numerical results give the same critical exponents, ν , and β , for all n and agree with MF predictions (for β and ν). The exponents appear to be universal, i.e., independent of the coupling parameter, β .

Deviations from MF in general grow with diminishing dimension [12]. The two-dimensional analogue of the counterion-cylinder system consists of logarithmically interacting mobile counterions and a central charged disk. The 2D Hamiltonian reads $H_N = 2 \sum_{i=1}^N \ln r_i + 2 \sum_{i < j} \ln(|\mathbf{r}_i - \mathbf{r}_j|)$. Unlike in 3D, ν and β are related due to electroneutrality as $\nu = \beta N$. Thus the striking feature in 2D is that for a given Manning parameter, ξ , the coupling parameter tends to zero, $\beta \rightarrow 0$, in the limit of many counterions, $N \rightarrow 1$, and MF should become exact. Fig. 3a shows the simulated order parameter S_1 in 2D. For $N = 1$, the data trivially follow the SC prediction (5), dashed curve, and for increasing N , they tend to the MF prediction (4), solid curve. Accordingly, scaling analysis of the condensation threshold and the critical exponents for $N \rightarrow 1$ gives identical results as in 3D and thus no deviations from MF. However, closer inspection of the 2D data in Fig. 3a reveals a peculiar set of cusp-like singularities for finite N . In fact, these singularities correspond to delocalization events of individual counterions, which give rise to a sawtooth-like structure for mean energy and a series of discrete

peaks for heat capacity (Figs. 3b, c). This can be understood by a simple analysis of the 2D partition function: Suppose that $N - m$ counterions are firmly bound to the central cylinder (disk), while $m - 1$ counterions have evaporated to infinity ($m = 1; \dots; N$). Neglecting the delocalized ions, the partition function can be written as $Z_N = \int \prod_{i=m+1}^N d^2 \mathbf{x}_i \exp(-H_{N-m}) Z_N^{(m)}$, where $Z_N^{(m)} = \int d^2 \mathbf{x} \exp[2 \ln \mathbf{x} + \frac{2}{N} \sum_{i=m+1}^N \ln(|\mathbf{x}_i - \mathbf{x}|)]$ is the contribution from the m -th counterion which is assumed to be weakly localized. It is thus de-correlated from the firmly bound ions and $Z_N^{(m)}$ approximately factorizes as $Z_N^{(m)} = \int d^2 \mathbf{x} \exp[2 \ln \mathbf{x} + (2 - \beta N) \sum_{i=m+1}^N \ln |\mathbf{x}_i|] e^{(2 - \beta N) \ln \mathbf{x}}$. In the limit $\beta \rightarrow 1$, $Z_N^{(m)}$ diverges for Manning parameters $\xi = N - m$. For N counterions this gives a discrete set of singularities at $\xi = N - m$ with diverging heat capacity $C \sim (\xi - N - m)^{-2}$, and in agreement with our simulations (Fig. 3). For a Manning parameter range $N - (m + 1) < \xi < N - m$, there are m de-condensed ions. In the thermodynamic limit $N \rightarrow 1$, the fraction of de-condensed ions, m/N , becomes a smooth function and tends to the MF prediction [1, 3], i.e., $m/N \rightarrow 1 - \xi$.

In summary, both in 2D and 3D the location and critical exponents of the counterion-condensation transition at charged cylinders are correctly described by mean-field theory. The heat capacity is experimentally accessible: in 2D (parallel charged polymers), it consists of a discrete set of peaks at which single counterions condense, and in the limit $N \rightarrow 1$, it converges to the 3D shape with a universal jump at the condensation threshold.

Discussions with H. Boroudjerdi, Y. Burak, H. Örlund, Y. Y. Suzuki and support from the DFG (SFB-486) are acknowledged.

- [1] G. S. Manning, J. Chem. Phys. 51, 924 (1969); Ber. Bunsenges. Phys. Chem. 100, 909 (1996).
- [2] T. Alfrey, P. W. Berg and H. Morawetz, J. Polym. Sci. 7, 543 (1951); R. M. Fuoss, A. Katchalsky and S. Lifson, Proc. Natl. Acad. Sci. USA 37, 579 (1951).
- [3] M. LeBret and B. H. Zimm, Biopolymers 23, 287 (1984).
- [4] J. W. Klein and B. W. Are, J. Chem. Phys. 80, 1334 (1984).
- [5] A. Popov and D. A. Hoagland, J. Polym. Sci. Part B: Polym. Phys. 42, 3616 (2004).
- [6] P. Ander and M. Kardar, Macromolecules 17, 2431 (1984); L. M. Peña el and T. A. Litovitz, J. Chem. Phys. 96, 3033 (1992).
- [7] R. Das et al., Phys. Rev. Lett. 90, 188103 (2003).
- [8] M. Deseemo, C. Holm and S. May, Macromolecules 33, 199 (2000).
- [9] Q. Liao, A. V. Dobrynin and M. Rubinstein, Macromolecules 36, 3399 (2003).
- [10] A. Deshkovski, S. Obukhov and M. Rubinstein, Phys. Rev. Lett. 86, 2341 (2001); B. O'Shaughnessy and Q. Yang, ibid. 94, 048302 (2005); M. Henle, C. Santangelo, D. Patel and P. Pincus, Europhys. Lett. 66, 284 (2004); M. Muthukumar, J. Chem. Phys. 120, 9343 (2004).
- [11] A. Kholodenko and A. Beyerlein, Phys. Rev. Lett. 74, 4679 (1995); Y. Levin, Physica A 257, 408 (1998); Y. Y.

- Suzuki, J. Phys.: Condens. Matter 16, S2119 (2004).
- [12] J. Cardy, Scaling and Renormalization in Statistical Physics (Cambridge University Press, Cambridge, 1996).
- [13] J. DeRouchey, R. R. Netz and J. O. Radler, Eur. Phys. J. E 16, 17 (2005).
- [14] R. Sperb, Mol. Simul. 20, 179 (1998).
- [15] A. G. Moreira and R. R. Netz, Europhys. Lett. 52, 705 (2000); Eur. Phys. J. E 8, 33 (2002).
- [16] A. Najj and R. R. Netz, to be published.